Article

A Tunable Broadband Terahertz Absorber Based on Plasmon Hybridization in Monolayer Graphene Ring Arrays

Dan Hu [1,] *, Tianhua Meng [2], Hongyan Wang [3] and Yongkang Ma [3]

[1] School of Physics and Electrical Engineering, Anyang Normal University, Anyang 455000, China;
[2] Department of Physics and Electronics Science, Shanxi Datong University, Datong Shanxi 037009, China; mengtianhua@sxdtdx.edu.cn (T.M.)
[3] School of Education Information Technology and Communication, Anyang Normal University, Anyang 455000, China; w_hy123@163.com (H.W.); 1278964464@qq.com (Y.M.)
* Correspondence: tylzhd@163.com; Tel.: +86-18738222875 (D.H.)

Abstract: Graphene as a new two-dimensional material can be utilized to design tunable optical devices owing to its exceptional physical properties such as high mobility and tunable conductivity. In this paper, we present the design and analysis of a tunable broadband terahertz absorber based on periodic graphene ring arrays. Due to plasmon hybridization modes excited in the graphene ring, the proposed structure achieves a broad absorption bandwidth with more than 90% absorption in the frequency range of 0.88-2.10THz under normal incidence and its relative absorption bandwidth is about 81.88%. Meanwhile, it exhibits polarization-insensitive behavior and maintains high absorption over 80% when incident angle is up to 45º for both TE and TM polarizations. Additionally, the peak absorption rate of the absorber can be tuned from 21% to nearly 100% by increasing the graphene's chemical potential from 0eV to 0.9eV. Such a design can have some potential applications in various terahertz devices, such as modulators, detectors, spatial filters.

Keywords: metamaterial; graphene; terahertz; broadband absorber

1. Introduction

Terahertz (THz) wave, as an important part of electromagnetic spectrum family, is located between microwave and infrared region with the frequency range of 0.1-10THz [1]. In the past twenty years, THz technology has become one of the most attended research fields owing to its potential applications in public security, communication, nondestructive detection and so on [2]. However, the lack of high-performance functional devices, such as modulators, wave plates, perfect absorbers, has seriously hindered development and application of THz technology. Among these functional devices, perfect absorbers are highly desirable for manipulating THz wave in many important application areas.

Many efforts have been made to develop perfect THz absorbers based on metamaterials [3-5]. In recent years, metamaterial perfect absorbers (MPAs) have become one of the most popular research hotspots and get rapid development in operating frequency and working bandwidth [6-9]. However, these MPAs with a sandwich structure consisted of metal-dielectric-metal are passive devices and have no capacity for real-time adjustment. To solve this issue, several design approaches have been carried out including micro electro mechanical system (MEMS) [10, 11], optical [12, 13], thermal [14], and electrical [15]. Although these methods have made great progress, there are still some limitations, such as less bandwidth, complex operation.

Graphene, a two-dimensional (2D) material consisted of a single flat sheet of carbon atoms arranged in a honeycomb lattice, has become one of the attractive materials due to its excellent and unique properties in high electron mobility, tunable conductivity, high optical transparency [16]. The

combination of these unique properties make graphene promising candidate for application in active optoelectronics applications and absorber devices [17-19]. Recently, various graphene MPAs have been reported at THz frequencies [18-25], but most of them were narrow in absorption band. To broaden absorption bandwidth, lots of graphene MPAs with a gradient width graphene pattern [26, 27], coplanar multiple graphene patterns [28-31], stacked multilayer graphene patterns [32-37], composite graphene-metal or graphene-dielectric patterns [38-40], have also been proposed. However, many of these absorbers suffer from some drawbacks, such as complex structure, polarization/angle sensitive, which greatly limit their practical applications. Therefore, the effective design of a MPA with broadband, polarization-insensitive, wide-angle, and simple structure is highly desirable for THz applications.

In this paper, we propose a novel broadband and tunable MPA, which is constructed by a simple graphene ring. Thanks to the effectively excited of hybrid plasmon resonances in the graphene ring, a relative bandwidth of more than 90% absorption can reach up to 81.88% at THz frequencies. Additionally, the peak absorptivity of this absorber can be actively tuned from 21% to nearly 100% by controlling the graphene's chemical potential from 0eV to 0.9eV. Meanwhile, the proposed MPA is polarization-insensitive and also exhibits well performance within a wide incident angle. Compared with those graphene-based broadband MPAs mentioned above, the value of this work is that we reveal the polarization-insensitive and wide-angle broadband absorption performance in a much simpler and flexible graphene-based ring structure.

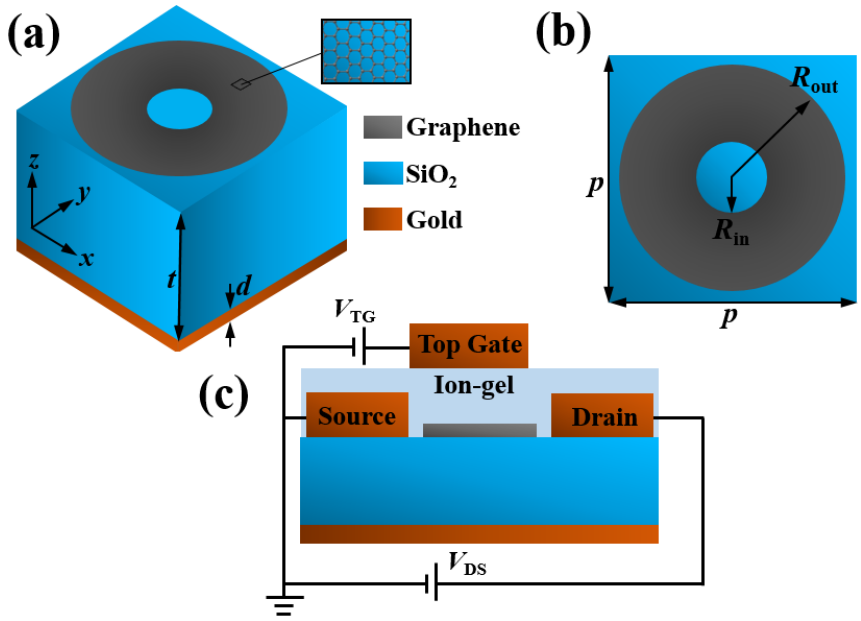

Figure 1 (a) Schematic view of the unit-cell structure of the proposed MPA. (b) Top view of the unit-cell structure. (c) Schematic view of top gate structure tuning graphene chemical potential.

2. Materials and Methods

The schematic view of the unit-cell structure of the proposed MPA is displayed Figs. 1(a) and 1(b). It is composed of a single-layer graphene ring array separated by a thin SiO_2 dielectric film, which is served as the insulating spacer with relative permittivity of 3.9 [19], and a gold plate with a conductivity of σ=4.56×10^7 S/m at the bottom is used as the ground plane to block the transmission [40]. The optimal geometric parameters of the proposed MPA are given as: d=1mm, t=25mm, R_{in}=5μm, R_{out}=16μm, p=35μm. The conductivity (σ_g) of the graphene can be calculated by using the Kubo formula [41]:

$$\sigma_g(\omega)=\frac{ie^2k_BT}{\pi\hbar(\omega+i\tau^{-1})}\left[\frac{\mu_c}{k_BT}+2\ln(e^{\frac{-\mu_c}{k_BT}}+1)\right]+\frac{ie^2}{4\pi\hbar}\ln\left[\frac{2|\mu_c|-\hbar(\omega+i\tau^{-1})}{2|\mu_c|+\hbar(\omega+i\tau^{-1})}\right] \quad (1)$$

where, e is the electron charge, k_B is the Boltzmann constant, $\hbar$ is the reduced Plank constant, ω is the angular frequency, τ is the relaxation time, μ_c is the chemical potential, and T is the temperature in Kelvin. In this paper, the relaxation time τ is set to be 0.1ps, T=300K, and the chemical potential μ_c can be tuned by the top gate method [42], as shown in Fig. 1(c).

The simulations are carried out by employing the frequency domain solver in CST Microwave Studio. Floquet ports are applied in z-direction and unit cell boundary conditions are applied in x- and y-directions. In this simulation, the single-layer graphene sheet is modeled as an equivalent 2D surface impedance layer (Z=1/σ_g) with zero thickness [29]. The initial value of the graphene chemical potential is assumed to be μ_c=0.9eV. The reflection $R(\omega)$ and transmission $T(\omega)$ are obtained from the frequency-dependent S-parameters, that is, $R(\omega)=|S_{11}(\omega)|^2$ and $T(\omega)=|S_{21}(\omega)|^2$. The absorption $A(\omega)$ is calculated as $A(\omega)=1-R(\omega)-T(\omega)$. The transmission $T(\omega)$ is close to zero at the studied frequency range since the gold ground plane is thick enough.

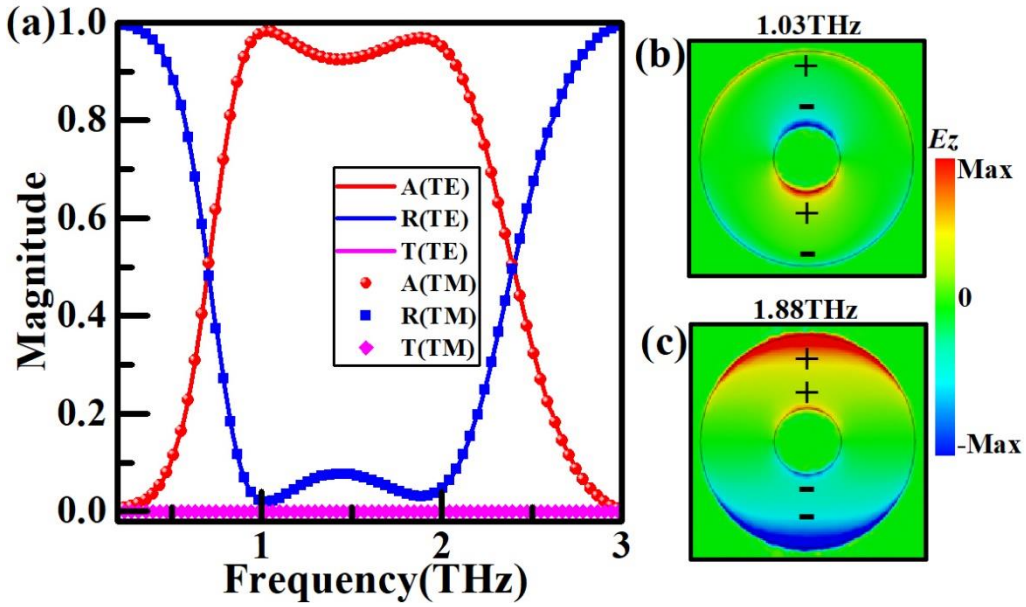

Figure 2 (a) The reflection, transmission, absorption spectra of the proposed MPA. The distributions of electric field E_z (in the xoy plane) at frequencies of 1.03THz (b) and1.88THz (c).

3. Results and discussion

To investigate the absorption performance of the proposed MPA, the reflection, transmission, and absorption spectra of the proposed MPA are simulated for both TE (the electric field is parallel to y-direction) and TM (the magnetic field is parallel to y-direction) polarizations under normal incidence, as shown in Fig. 2(a). From the figure, one sees that the transmission is almost zero due the thick gold ground plane, and the absorption spectra for both TE and TM polarizations are coincident with each other. Furthermore, we can find that there are two close resonance frequencies (f_1=1.03THz and f_2=1.88THz), thus forming a broadband absorption property of over 90% in the frequency range from 0.88THz to 2.10THz with a relative bandwidth of 81.88%, which is much larger than that reported in [26-30, 34, 38-40]. Figs. 2(b) and 2(c) show the z-component electric field (E_z) distributions at the modes f_1 and f_2 for TE polarization, respectively. We can observe from the charge distribution patterns that the two resonances are originated from the typical hybridization of plasmons [43, 44]; namely, the resonance at mode f_1 is due to the dipolar anti-bonding resonance mode or high-order dipolar bonding resonance mode [see Fig. 2(b)], while the other resonance at mode f_2 is attributed to the dipolar bonding resonance mode [see Fig. 2(c)].

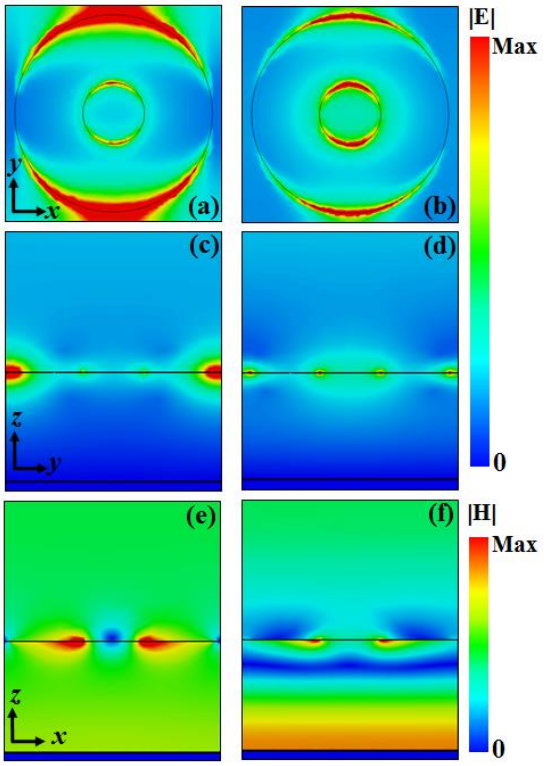

Figure 3 The distributions of the electric field |*E*| [in the *xoy* (a, b), and *yoz* (c, d) planes] and magnetic field |*H*| [in the *xoz* plane (e, f)] at the frequencies of f_1=1.03THz and 1.88THz, respectively.

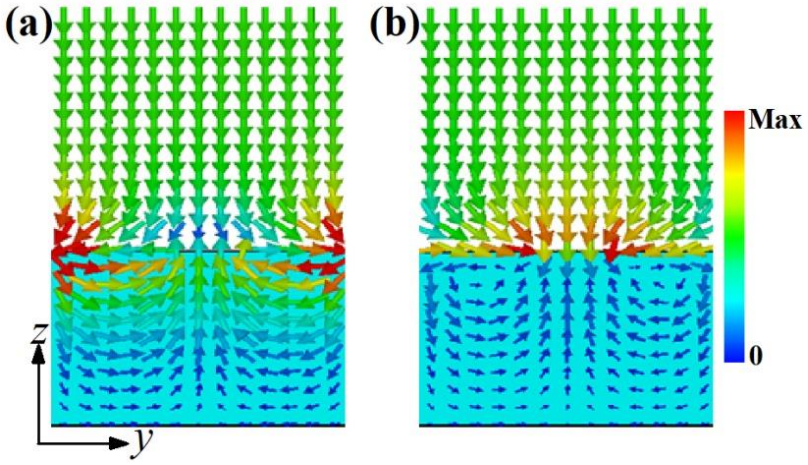

Figure 4 The distribution of power flow in the *yoz* plane of the proposed MPA at frequencies of f_1=1.03THz (a), and f_2=1.88THz (b).

To further understand the underlying physical mechanism behind the two near-perfect resonance absorption peaks, in Fig. 3 we give the distributions of the electric and magnetic fields for TE polarization. At mode f_1, the electric field |*E*| is mainly distributed on the outer edges of the graphene ring and the space between adjacent unit cells and a small fraction on the inner edges of the graphene ring [see Figs. 3(a) and 3(c)]. At mode f_2, it is mainly assembled at the inner and outer edges of the graphene ring [see Figs. 3(b) and 3(d)]. Based on the electric field distribution at different resonance modes, this demonstrates here that the resonance absorption of the proposed MPA is induced by the graphene ring resonator. From Fig. 3(e) and 3(f), one can see that the magnetic fields are distributed in the SiO_2 spacer region between the graphene ring and the gold ground plane. The field distribution properties demonstrate the excitation of magnetic dipolar resonance. In general, the synergy of magnetic resonance, dipolar resonance with interaction between neighboring cells lead to

the broadband perfect absorption in the THz region. The situation is the same for TM polarization since the proposed graphene ring is asymmetry structure

In addition, it is very necessary to give the power flow distribution since it can give further insight into how and where the absorption happens in the absorber structure. The power flow distributions of *yoz* plane at the two resonance modes f_1 and f_2 are as shown in Figs. 4(a) and 4(b), respectively. For mode f_1, most of streams flow across the space between the neighboring graphene rings, then curl in the dielectric layer, and finally concentrate on the inner ring region of the graphene ring. However, for mode f_2, most of streams flow across the inner ring region of the graphene ring, curl in the dielectric layer, and ultimately back into the inner ring region of the graphene ring. These results demonstrate that the energy of the incident THz wave can be confined at specific positions of the absorber structure and is finally absorbed.

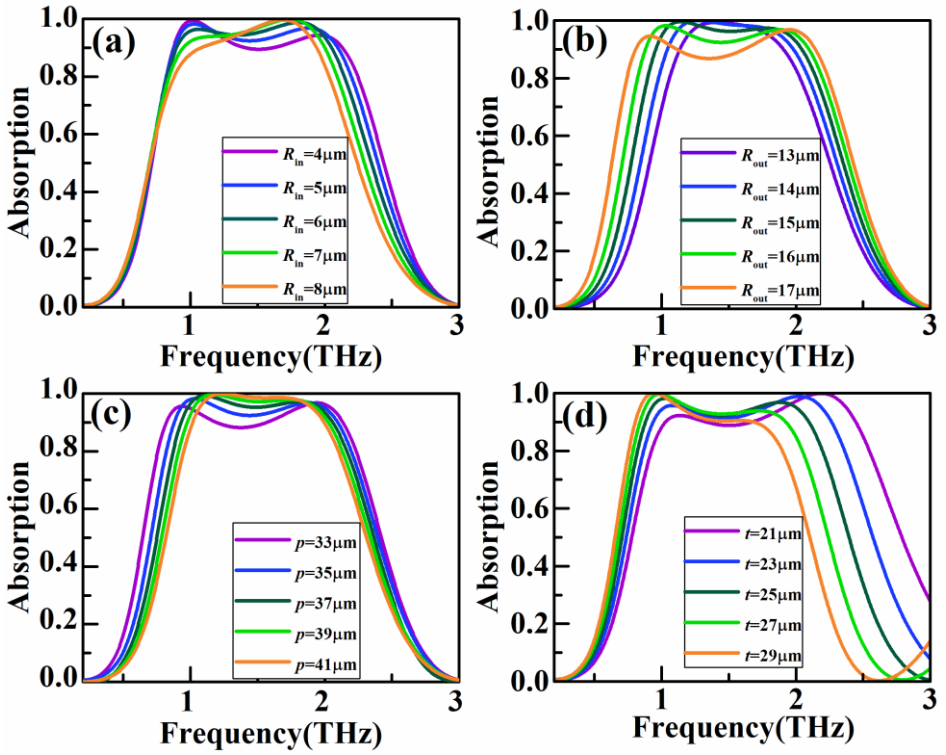

Figure 5 Absorption spectra of the proposed MPA with different inner radius R_{in} (a), outer radius R_{out} (b) of the graphene ring, period of unit cell p (c), and thickness of dielectric spacer t (d).

Next, we investigate the influences of the geometrical parameters (R_{in}, R_{out}, p, and t) on the absorption spectra of the proposed MPA. Fig. 5(a) shows the absorption spectra of the proposed MPA with different inner radii (R_{in}) of the graphene ring. It is clear that the mode f_1 slightly increases with increasing R_{in}, while the mode f_2 decreases. For the mode f_1, when increasing R_{in}, not only the localized field between the adjacent cells will weaken resulted from the opposite directions of attractive force in the graphene ring, but also the effectively distance between the opposite charges will decrease, thus leading to the slightly increase of the mode f_1. For mode f_2, its resonance frequency can be obtained by the equation [37, 45]: $2\pi R\sqrt{\varepsilon_{eff}} = mc/f$, where ε_{eff} is the effective dielectric constant of the substrate, R= (R_{in}+R_{out})/2 is the average radius of the graphene ring, m is the resonance order, c is the speed of light in vacuum, and f is the resonance frequency. From the equation we can know that the mode f_2 decreases with the increase of R_{in}. Fig. 5(b) shows the effect of the outer radius (R_{out}) on the absorption spectra of the proposed MPA. Based on the mentioned analysis, we can know that the mode f_1 decreases with the increase of R_{out}. Interestingly, the mode f_2 increases with the increase of R_{out}. That is because the dipolar bonding resonance will attract the mode f_2 to decrease when increasing R_{out}, but the interaction between the adjacent cells will drive the mode f_2 to increase, which eventually causes the mode f_2 to increase. The explanation can be confirmed by changing the

period of unit cell. Fig. 5(c) shows the absorption spectra of the proposed MPA with different periods (p). With the change of p, the modes f_1 and f_2 show an opposite shift, which is due to the interaction of neighboring cells [46, 47]. Note that although the two modes narrow the absorption bandwidth with the increase of p, it can exhibit a broad and flat high absorption band, which is very useful for many practical applications. For example, when p=41 m, the proposed MPA can reach nearly perfect broadband absorption with more than 95% absorption from 1.07 to 1.91THz, corresponding to the relative bandwidth of 56.37%. In addition, we also study the effect of the thickness of the dielectric spacer (t) on the absorption spectra of the proposed MPA, as shown in Fig. 5(d). It can be seen from the Fig. 5(d) that both the modes f_1 and f_2 decrease with the increase of t, which is can be explained well by the effective capacitance between the graphene ring and the gold ground plane, and impedance matching with the free space [48].

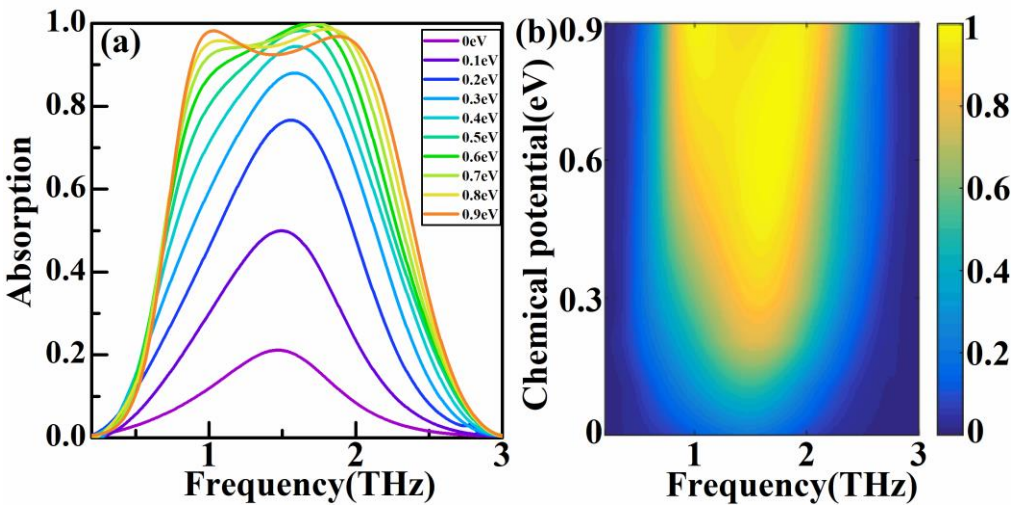

Figure 6 The absorption spectra of the proposed MPA with different chemical potential for TE and TM polarizations.

In addition, the tunability of the absorption spectra for TE and TM polarizations under normal incidence is studied, as shown in Fig. 6. Fig. 6 (a) shows the absorption spectra as a function chemical potential μ_c with different μ_c ranging from 0eV to 0.9eV for TE polarization. From Fig. 6(a) it is observed that the peak absorption rate can be continually tuned from 21% to nearly 100% when μ_c increases from 0eV to 0.9eV. Due to structure symmetry, the tunable absorption performances of the proposed MPA are the same for TE and TM polarizations. Here, the graphene chemical potential can be modulated by sol-gel top gating method [42].

In the practical applications, such as THz imaging, detecting and stealth technology, the absorption should be less dependence on the polarization angle and incident angle. Therefore, we first investigate the dependence of polarization angle on the absorption of the proposed MPA. As shown in Fig. 7(a), It is observed that the broadband absorption of the propose MPA stays fairly steady with the polarization angle φ changing from 0° to 90°. This indicates that it is polarization-independent resulted from the high-degree symmetry of the graphene ring. Figs. 7(b) and 7(c) show the dependences of absorption on the incident angle (θ) for both TE and TM polarizations, respectively. Obviously, the proposed MPA can exhibit excellent broadband absorption performance over a relatively wide range of incident angles. For TE polarization, it can be seen that the broadband absorption response (over 80%) is still achieved even when the θ is up to 45°, in the frequency range of 1.03THz to 2.09THz [see Fig. 7(b)]. For TM polarization, more than 90% and 80% absorption in the frequency range of 1.03 THz to 2.09THz can be observed when the θ is up to 50° and 60°, respectively [see Fig. 7(c)]. These demonstrate the proposed broadband MPA possesses polarization-independent and wide-angle properties, which will greatly increase its practicability in future THz device applications.

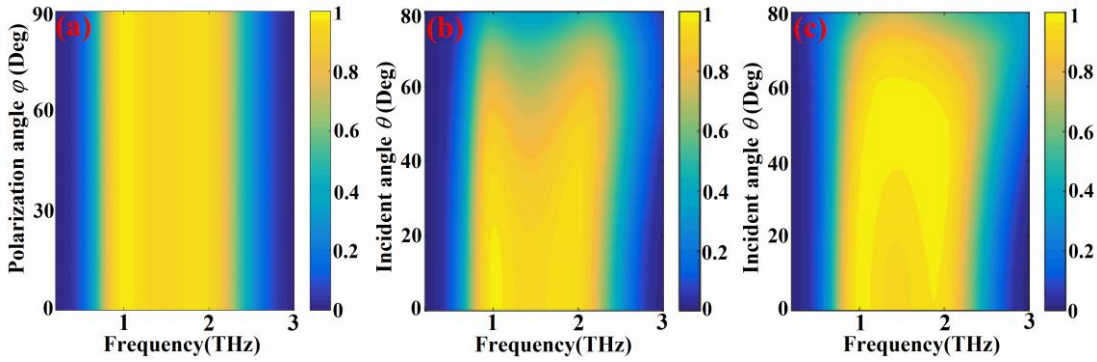

Figure 7 The absorption spectra of the proposed MPA with different polarization angle (a) and incidence angle for TE (b) and TM (c) polarizations.

4. Conclusions

In conclusion, we present a broadband MPA consisted of a graphene ring, a gold ground plane separated by a SiO_2 dielectric spacer. The proposed structure shows over 90% in the frequency range from 0.88THz to 2.10THz with the relative bandwidth of 81.88%. The broadband absorption characteristics are achieved by the synergy of dipolar resonances and magnetic response. The broadband perfect absorption of the proposed MPA also exhibits greatly insensitive to the incidence angle and polarization angle. The over 80% absorption in the frequency range of 1.03 THz to 2.09THz is still maintained over a wide incidence angle up to 45° for both TE and TM polarizations. In addition, the peak absorption rate can be continually tuned from 21% to nearly 100% by adjusting the graphene chemical potential from 0eV to 0.9eV. Thanks to the outstanding tunable capability and insensitive of the polarization angle and the angle of incidence, the proposed broadband MPA has tremendous potential for various applications, such as THz imaging, modulators, and attenuators.

Author Contributions: Conceptualization, D.H.; methodology, T.M..; software, Y.M.; validation, D.H., T.M., and H.W.; formal analysis, D.H.; investigation, Y.M.; resources, Y.M.; data curation, Y.M.; writing—original draft preparation, D.H.; writing—review and editing, D.H., T.M., H.W. and Y.M.; visualization, H.W.; supervision, D.H.; project administration, D.H.; funding acquisition, D.H., T.M. and H.W.; All authors have read and agreed to the published version of the manuscript.

Funding: The work supported by the National Natural Science Foundation of China (11504006, 61805072), the Key Scientific Research Project of Colleges and Universities in Henan Province (19A140002), the National College Students Innovation and Entrepreneurship Training Program (X2020104790161), and the Shanxi Provincial Key Research and Development Project (201803D121083).

Conflicts of Interest: The authors declare no conflict of interest.

References

1. Ferguson, B.; Zhang, X. C. Materials for terahertz science and technology. Nature Mater. **2002**, 1, 26-33.
2. Tonouchi, M. Cutting-edge terahertz technology. Nature Photon. **2007**, 1, 97-105.
3. Tao, H.; Landy, N. I.; Bingham, C. M.; Zhang, X.; Averitt, R. D.; Padilla W. J. A metamaterial absorber for the terahertz regime: design, fabrication and characterization. Opt. Express **2008**, 16, 7181-7188.
4. Grant, J.; Ma, Y.; Saha S.; Khalid, A.; Cumming, D. R. S. Polarization insensitive, broadband terahertz metamaterial absorber. Opt. Lett. **2011**, 36, 3476-3478.
5. Shen, X. P.; Yang, Y.; Zang, Y. Z.; Gu, J. Q.; Han, J. G.; Zhang, W. L.; Cui, T. J. Triple-band terahertz metamaterial absorber: Design, experiment, and physical interpretation. Appl. Phys. Lett. **2012**, 101, 154102.
6. Liu, S.; Chen, H. B.; Cui, T. J. A broadband terahertz absorber using multi-layer stacked bars. Appl. Phys. Lett. **2015**, 106, 151601.
7. Mao, Z. W.; Liu, S. B.; Bian, B.; Wang, B. Y.; Ma, B.; L. Chen; Xu, J. Y. Multi-band polarization-insensitive metamaterial absorber based on Chinese ancient coin-shaped structures. J. Appl. Phys. **2014**, 115, 204505.
8. Y. Z. Wen, W. Ma, J. Bailey, G. Matmon, X. M. Yu, G. Aeppli, Planar broadband and high absorption metamaterial using single nested resonator at terahertz frequencies. Opt. Lett. **2014**, 39, 1589-1592.

9. Hu, D.; Wang, H. Y.; Zhu, Q. F. Design of six-band terahertz perfect absorber using a simple U-shaped closed-ring resonator. IEEE Photon. J. **2016**, 8, 5500608.
10. Hu, F. R.; Xu, N. N.; Wang, W. M.; Wang, Y. E.; Zhang, W. T.; Han, J. G.; Zhang, W. L. A dynamically tunable terahertz metamaterial absorber based on an electrostatic MEMS actuator and electrical dipole resonator array. J. Micromech. Microeng. **2016**, 26, 025006.
11. Liu, M. K.; Susli, M.; Silva, D.; Putrino, G.; Kala, H.; Fan, S. T.; Cole, M.; Faraone, L.; Wallace, V. P.; Padilla, W. J.; Powell, D. A.; Shadrivov, I. V.; Martyniuk, M. Ultrathin tunable terahertz absorber based on MEMS-driven metamaterial. Microsyst. Nanoeng. **2017**, 3, 17033
12. Seren, H. R.; Keiser, G. R.; Cao, L. Y.; Zhang, J. D.; Strikwerda, A. C.; Fan, K. B.; Metcalfe, G. D.; Wraback, M.; Zhang, X.; Averitt, R. D. Optically modulated multiband terahertz perfect absorber. Adv. Opt. Mater. **2014**, 2, 1221-1226.
13. Zhao, X. G.; Wang, Y.; Schalch, J.; Duan, G. W.; Cremin, K.; Zhang, J. D.; Chen, C. X.; Averitt, R. D.; Zhang, X. Optically modulated ultra-broadband all-silicon metamaterial terahertz absorbers. ACS Photon. **2019**, 6, 830-837.
14. Wen, Q. Y.; Zhang, H. W.; Yang, Q. H.; Chen, Z.; Long, Y.; Jing, Y. L.; Lin, Y.; Zhang, P. X. A tunable hybrid metamaterial absorber based on vanadium oxide films. J. Phys. D: Appl. Phys. **2012**, 45, 235106.
15. Isić, G.; Vasić, B.; Zografopoulos, D. C.; Beccherelli, R.; Gajić, R. Electrically tunable critically coupled terahertz metamaterial absorber based on nematic liquid crystals. Phys. Rev. Appl. **2015**, 3, 064007.
16. Grigorenko, A.; Polini, M.; Novoselov, K. Graphene plasmonics. Nat. Photonics **2012**, 6, 749-758.
17. Avouris, P.; Freitag, M. Graphene photonics, plasmonics and optoelectronics. IEEE J. Sel. Top. Quant. Electron. **2013**, 20, 72-83.
18. Chen, X. Y.; Tian, Z.; Lu, Y. C.; Xu, Y. H.; Zhang, X. Q.; Ouyang, C. M.; Gu, J. Q.; Han, J. G.; Zhang, W. L. Electrically tunable perfect terahertz absorber based on a graphene salisbury screen hybrid metasurface. Adv. Opt. Mater. **2020**, 8, 1900660.
19. Hu, D.; Meng, T. H.; Wang, H. Y.; Zhang, X. W.; Tang, Z. J., Wang, Z., Zhu, Q. F. Tunable broadband terahertz absorber using a single-layer square graphene patch with fourfold rotationally symmetric groove. Opt. Mater. **2020**, 109, 110235.
20. Chen, P. Y.; Alù, A. Terahertz metamaterial devices based on graphene nanostructures. IEEE Trans. Terahertz Sci. Technol. **2013**, 3, 748-756.
21. Qi, Y. P.; Zhang, Y.; Liu, C. Q.; Zhang, T.; Zhang, B. H.; Wang, L. Y.; Deng X. Y.; Wan X. X.; Yu, Y. A tunable terahertz metamaterial absorber composed of hourglass-shaped graphene arrays. Nanomaterials **2020**, 10, 533.
22. Yao, G.; Ling, F. R.; Yue, J.; Luo, C. Y.; Ji, J.; Yao, J. Q. Dual-band tunable perfect metamaterial absorber in the THz range. Opt. Express **2016**, 24, 1518-1527.
23. Yi, Z.; Chen, J. J.; Cen, C. L.; Chen, X. F.; Zhou, Z. G.; Tang, Y. J.; Ye, X.; Xiao, S. Y.; Luo, W.; Wu, P. H. Tunable graphene-based plasmonic perfect metamaterial absorber in the THz region. Micromachines **2019**, 10, 194.
24. Sun, P.; You, C. L.; Mahigir, A.; Liu, T. T.; Xia, F.; Kong, W. J.; Veronis, G.; Dowling, J. P., Dong, L. F.; Yun, M. J. Graphene-based dual-band independently tunable infrared absorber. Nanoscale **2018**, 10, 15564-15570.
25. Sang, T.; Gao, J.; Wang, L.; Qi, H. L.; Yin, X.; Wang, Y. K.; Numerical study of angle-insensitive and tunable dual-band THz absorber using periodic cross-shaped graphene arrays. Materials **2019**, 12, 2063.
26. Zhu, Z. H.; Guo, C. C.; Zhang, J. F.; Liu, K.; Yuan, X. D.; Qin, S. Q. Broadband single-layered graphene absorber using periodic arrays of graphene ribbons with gradient width. Appl. Phys. Express **2015**, 8, 015102.
27. Ye, L. F.; Chen, Y.; Cai, G. X.; Liu, N.; Zhu, J. F.; Song, Z. Y.; Liu, Q. H. Broadband absorber with periodically sinusoidally-patterned graphene layer in terahertz range. Opt. Express **2017**, 25, 11223-11232.
28. Yi, S.; Zhou, M.; Shi, X.; Gan, Q. Q.; Zi, J.; Yu, Z. F. A multiple-resonator approach for broadband light absorption in a single layer of nanostructured graphene. Opt. Express **2015**, 23, 10081-10090.
29. Li, Y. J.; Wu, J.; Wang, C. W.; Shen, Z. Y.; Wu, D.; Wu, N.; Yang, H. L. Tunable broadband metamaterial absorber with single-layered graphene arrays of rings and discs in terahertz range. Phys. Scr. **2019**, 94, 035703.

30. Du, X. M.; Yan, F. P.; Wang, W., Tan, S. Y.; Zhang, L.; Bai, Z. Y.; Zhou, H.; Hou, Y. F. A polarization- and angle-insensitive broadband tunable metamaterial absorber using patterned graphene resonators in the terahertz band. Opt. Laser Technol. **2020**, **132, 106513.**
31. Ye, L. F.; Chen, X.; Cai, G. X.; Zhu, J. F.; Liu, Na; Liu Q. H. Electrically tunable broadband terahertz absorption with hybrid-patterned graphene metasurfaces. Nanomaterials **2018**, 8, 562.
32. Amin, M.; Farhat, M.; Bağcı, H. An ultra-broadband multilayered graphene absorber. Opt. Express **2013**, 21, 29938-29948.
33. Xu, Z. H.; Wu, D.; Liu, Y. M.; Liu, C.; Yu, Z. Y.; Yu, L.; Ye, H. Design of a tunable ultra-broadband terahertz absorber based on multiple layers of graphene ribbons. Nanoscale Res. Lett. **2018**, 13, 143.
34. Cai, Y. J.; Xu, K. D. Tunable broadband terahertz absorber based on multilayer graphene-sandwiched plasmonic structure. Opt. Express 2018, 26, 31693-31705.
35. Fardoost, A.; Vanani, F.; Safian, R. Design of a multilayer graphene-based ultrawideband terahertz absorber. IEEE Trans. Nanotechnol., **2016**, 16, 68-74.
36. Chen, D. B.; Yang, J. B.; Zhang, J. J.; Huang, J.; Zhang, Z. J. Tunable broadband terahertz absorbers based on multiple layers of graphene ribbons. Sci. Rep. **2017**, 7, 15836.
37. Qi, L. M.; Liu, C. Broadband multilayer graphene metamaterial absorbers. Opt. Mater. Express **2019**, 9, 1298-1309.
38. Yang, J. W.; Zhu, Z. H.; Zhang, J. F.; Guo, C. C.; Xu, W.; Liu, K.; Yuan, X. D.; Qin, S. Q. Broadband terahertz absorber based on multi-band continuous plasmon resonances in geometrically gradient dielectric loaded graphene plasmon structure. Sci. Rep. **2018**, 8, 3239.
39. Nejat, M.; Nozhat, N. Design, theory, and circuit model of wideband, tunable and polarization-insensitive terahertz absorber based on graphene. IEEE Trans. Nanotech., **2019**, 18, 684-690.
40. Han, X.; Qing, J.; Tahir, B.; Fan, Y. Dual-controlled broadband terahertz absorber based on graphene and Dirac semimetal. Opt. Express **2020**, 28, 13884-13894.
41. Hanson, G. W. Dyadic Green's functions and guided surface waves for a surface conductivity model of graphene. J. Appl. Phys. **2008**, 103, 064302.
42. Chen, C. F.; Park, C. H.; Boudouris, B. W.; Horng, J.; Geng, B.; Girit, C.; Zettl, A.; Crommie, M. F.; Segalman, R. A.; Louie, S. G.; Wang, F. Controlling inelastic light scattering quantum pathways in graphene. Nature **2011**, 471, 617-620.
43. Prodan, E.; Radloff, C.; Halas, N. J.; Nordlander, P. A hybridization model for the plasmon response of complex nanostructures. Science **2003**, 302, 419-422.
44. Mou, N. L.; Sun, S. L.; Dong, H. X.; Dong, S. H.; He, Q.; Zhou, L.; Zhang, L. Hybridization-induced broadband terahertz wave absorption with graphene metasurfaces. Opt. Express **2018**, 26, 11728-11736.
45. Cen, C. L.; Zhang, Y. B.; Chen, X. F.; Yang, H.; Yi, Z.; Yao, W. T.; Tang, Y. J.; Yi, Y. G.; Wang, J. Q.; Wu, P. H. A dual-band metamaterial absorber for graphene surface plasmon resonance at terahertz frequency. Phys. E **2020**, 117, 113840.
46. Le, K. Q.; Bai, J. Enhanced absorption efficiency of ultrathin metamaterial solar absorbers by plasmonic Fano resonance, J. Opt. Soc. Am. B **2015**, 32, 595-600.
47. Wang, B. X., Wang, L. L., Wang, G. Z., Huang, W. Q., Li, X. F., Zhai, X. A simple design of a broadband, polarization-insensitive, and low-conductivity alloy metamaterial absorber. Appl. Phys. Express **2014**, 7, 082601.
48. Zhang, Q. F.; Ma, Q. X.; Yan, S. T.; Wu, F. M.; He, X. J.; Jiang, J. X. Tunable terahertz absorption in graphene-based metamaterial. Opt. Commun. **2015**, 353, 70-75.